A Molecular Simulation Study of Adsorption and Desorption in Closed End Slit Pores

Is There a Hysteresis Loop?

by

Chunyan Fan[+], Yonghong Zeng, D. D. Do* and D. Nicholson
[+] Department of Chemical Engineering
Curtin University
Bentley, Perth 6845
Australia

School of Chemical Engineering
University of Queensland
St. Lucia, Qld 4072
Australia

Abstract

This paper reports detailed simulations of adsorption and desorption of argon in closed end slit pores with the aim of investigating the existence of hysteresis. The classical thermodynamic approach implies that there should be no hysteresis in a closed end pore because it assumes that the condensed phase is identical to a uniform bulk liquid and that the interface between the gas-like region and the dense adsorbate region is the same when the pore fills as when it empties. Our simulations show that hysteresis is possible and we support this assertion with evidence from a critical analysis of the classical equation. Our extensive results show that hysteresis can occur in closed end pores because of the continuous structuring of the adsorbed phase induced by the combined effects of the solid-fluid interaction and the fluid-fluid interaction.

* Author to whom all correspondence should be addressed. Email: d.d.do@uq.edu.au

A contribution to the Special Issue on Molecular Simulation in Chemical Engineering Science Journal.
Guest Editor: Professor Mark Biggs.

1. Introduction

Adsorption isotherms for gases in meso-porous adsorbents exhibit hysteresis at temperatures below a critical hysteresis temperature, T_{ch} (Everett and Haynes, 1973; Horikawa et al., 2011; Thommes, 2004) which depends on the parameters characterising the adsorbent pores (cross sectional shape and width, inter-connectivity, and the form of the adsorbent-adsorbate potential) and also on the adsorbate. The drive to improve our understanding of the microscopic origin of hysteresis has been greatly facilitated by the synthesis of ordered mesoporous solids and advances in computer simulation (Horikawa et al., 2011). Several attempts have been made to tailor adsorbent solids in order to study the dependence of hysteresis on pore structure, for example by synthesising pores with either open ends, or with one end closed, or pores with narrower openings to the surrounding gas (Bruschi et al., 2008; Bruschi et al., 2010; Wallacher et al., 2004). In particular, the possible existence of hysteresis in closed end pores has been a controversial topic that has important consequences for more complex materials where pore cross sections may vary from place to place. The classical Kelvin equation implies that there would be no hysteresis in a cylindrical closed end pore because it assumes that the condensed phase is identical to a uniform bulk liquid and that the interface separating the gas-like region and the dense adsorbate region is the same when the pore fills as when it empties. In slit pore geometry this interface would be cylindrical rather than hemispherical, but a similar classical argument would apply. The assumption that the adsorbate resembles the bulk fluid has never been verified experimentally, and it is shown in this paper that this is the principal reason for the failure of the classical equation in the analysis of adsorption in closed end pores. Our simulations show that there is a continuous re-structuring of the adsorbed phase as adsorption progresses which is controlled by the strength of the solid-fluid interaction.

Experimental studies have shown conflicting results: for example isotherms in aluminium and silicon adsorbents with closed end pores exhibit hysteresis loops (Bruschi et al., 2008; Coasne et al., 2002; Wallacher et al., 2004). However, these real materials may have irregularities on the surface that could be responsible for the hysteresis (Bruschi et al., 2008; Puibasset, 2009). In an experimental adsorption study of very wide closed end pores where effects due to the external adsorbent field are expected to be negligible, no hysteresis was found (Mistura et al., 2013).

Theoretical studies using DFT or lattice model calculations have tended to the view that hysteresis does not occur in closed end pores (Parry et al., 2007; Roth and Parry, 2011), or may be attributed to irregularities in the pore walls (Naumov et al., 2009). Similarly, computer simulation studies have not reached a conclusive agreement because of their limited exploration of the parameter space. Sarkisov and Monson used molecular dynamics (MD) and Grand Canonical Monte Carlo (GCMC) to study adsorption in slit pores with closed ends but did not find hysteresis in the models they examined (Sarkisov and Monson, 2001) a conclusion supported by Wallacher et al and by Bruschi et al (Bruschi et al., 2010; Puibasset, 2009). On the other hand, Ancilotto *et al*. (Ancilotto et al., 2011), in their simulation study of cylindrical pores with closed ends, did find hysteresis but attributed this to the formation of a thin film of adsorbate spanning across the pore mouth. Our recent Monte Carlo simulations (Fan et al., 2013; Nguyen et al., 2013) of adsorption in closed-end cylindrical and slit pores, also reveal the existence of a hysteresis loop in these models, but without the need to invoke this explanation.

In this paper we explore the effects of various parameters on the existence and properties of the hysteresis loop in closed end pores. A number of the simulations discussed here have been presented in our previous correspondence, and are supplemented by new results which together present a comprehensive picture of the factors affecting hysteresis in closed end pores.

2. Theory

2.1 Interaction energies and pore models

We used argon as a model adsorbate and its intermolecular potential energy of interaction was described by the 12-6 Lennard-Jones (LJ) equation, with a collision diameter σ_{ff} = 0.3405nm and a reduced well-depth ε_{ff}/k = 119.8K.

The model was a slit-like pore with finite walls in the *y*-direction and infinite walls in the *x*-direction; one end of the pore was closed and the open end was connected to a bulk gas reservoir to ensure mechanical equilibrium between the pore and the surroundings (Figure 1). The pore walls including the closed end consisted of three homogeneous graphene layers with a constant surface density of 38.2nm^{-2} and a spacing $\Delta = 0.3354$ nm. The solid-fluid potential energy was calculated from the Bojan-Steele equation (Bojan and Steele, 1988;

Bojan and Steele, 1993; Bojan and Steele, 1998) with molecular parameters σ_{ss} = 0.34nm and ε_{ss}/k = 28K to represent a carbon atom. The cross collision diameter and well-depth of the solid-fluid interaction energy were calculated by the Lorentz-Berthelot mixing rule.

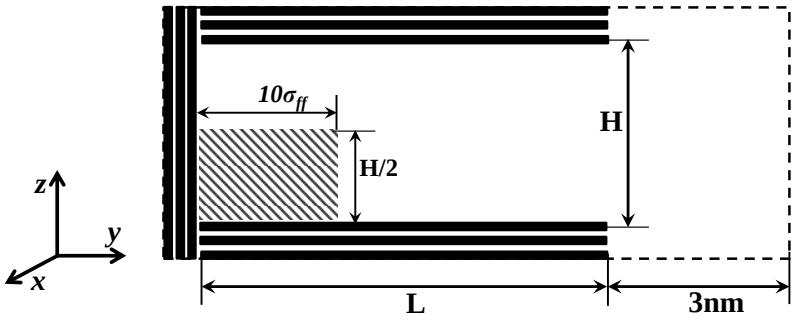

Figure 1: Schematic of the closed-end slit-shaped pore. The pore width H is defined as the distance between the planes passing through the centres of carbon atoms in the outermost layer of one wall to the corresponding plane of the opposite wall. The *x*-direction is perpendicular to the page.

2.2 Monte Carlo simulation

We used GCMC simulation to obtain isotherms, with 200,000 cycles in both the equilibration and sampling stages. Each cycle consisted of 1,000 displacement moves and exchanges with equal probability, giving a total of 2×10^8 configurations, which was found to be adequate to achieve convergence. A few simulations with much longer Markov chains yielded identical results. In the equilibration stage, the maximum displacement length was initially set as half of the largest dimension of the box and was adjusted at the end of each cycle to give an acceptance ratio for displacement of 20% (Mountain and Thirumalai, 1994). The dimension of the simulation box in the *x*-direction was set at 10 times the collision diameter of argon and the other two directions were determined by the pore size *H* and length *L*. The gas reservoir had a length along the pore axis of 3nm, and the dimensions in the other two directions were the same as those of the pore. Periodic boundary conditions were applied at the boundaries in the *x*- direction, and the cut-off radius was 5 times the collision diameter (which is half the dimension in that direction). The equation of state of Johnson *et al.* (Johnson et al., 1993) was used to relate pressure to the chemical potential, which was the input in GCMC simulation.

2.3 Mesoscopic analysis

The local density distribution in the *z*-direction from one of the pore walls is calculated from:

$$\rho(z) = \frac{\langle \Delta N(z) \rangle}{L_x L_y \Delta z} \tag{1}$$

where $\Delta N(z)$ is the number of molecules with centres in the bin bounded by $[z, z + \Delta z]$. For the 2D-density distribution, the system was divided into bins in the *z*- and *y*-directions and the bin density is defined as:

$$\rho(z, y) = \frac{\langle \Delta N(z, y) \rangle}{L_x \Delta z \Delta y} \tag{2}$$

where $\Delta N(z, y)$ is the number of particles in the bin bounded by $[z, z + \Delta z]$ and $[y, y + \Delta y]$. The bin size in both directions was chosen to be $\Delta z = \Delta y = 0.1\sigma_{ff}$. The local density was calculated at the end of each cycle, and the ensemble average obtained at the end of the sampling stage. The results of 2D-density profile were smoothed by averaging the density within a radius of $0.5\sigma_{ff}$.

We also calculated the radial density distribution for molecules in the corners of the pore in order to examine any structural changes in the adsorbate in the neighbourhood of the closed end.

$$\rho(r) = \frac{\langle \Delta N(r) \rangle}{\frac{4}{3}\pi\left[(r + \Delta r)^3 - r^3\right]} \tag{3}$$

where $\Delta N(r)$ is the number of particles in the radial bin bounded by $[r, r + \Delta r]$ and the denominator is its volume. The bin size was chosen as $\Delta r = 0.1\sigma_{ff}$. The selected corner region of the pore is shown in Figure 1 as a shaded area.

3. Results and Discussion

3.1 Open and Closed End Pore at 87.3K

The comparison between isotherms for argon adsorption at 87K in the open end and closed end slit pores constructed from homogeneous solid are presented in Figure 2; their widths and lengths are 3nm and 20nm, respectively. Although both hysteresis loops are of Type H1 according to the IUPAC classification, there are distinct differences between the two isotherms listed below. For ease of discussion, we denote the open and closed end pores as *O* and *C* respectively.

1. The loop for the *O*-pore is significantly larger

2. The condensation in the *O*-pore occurs at a higher pressure than the pressure at which the onset of the sharp change in density in the *C*-pore occurs.
3. The evaporation from the *O*-pore occurs at a pressure only slightly greater than the evaporation of the *C*-pore.
4. The adsorbate density in the *C*-pore is greater than in the *O*-pore at all pressures.

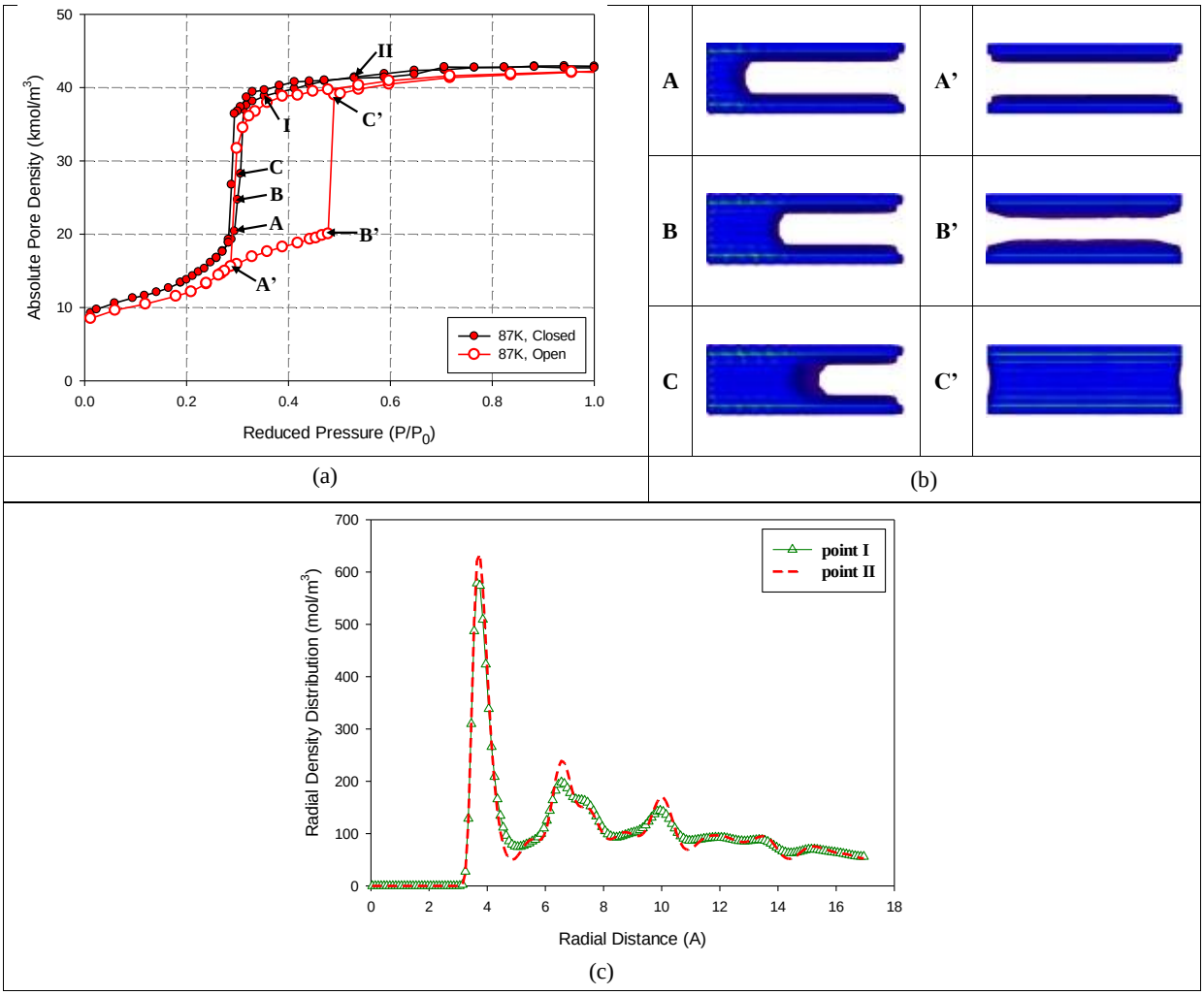

Figure 2: (a) The adsorption isotherms of argon at 87K adsorption in the *O*- and *C*-slit pores; the pore widths are 3nm and lengths are 20nm. (b) The 2D density profiles at the points labelled in (a); (c) The radial density distributions at points I and II in (a).

The explanations of these observations are as follows:

Point 1: The loop of *O*-pore is larger because the interface shapes in adsorption and desorption are different; a larger pressure is required to build up an adsorbed layer thick enough for condensation to occur, while desorption follows a process of withdrawal of the menisci from the pore mouths towards the pore interior in the *y*-

direction. The interface is the same shape in adsorption and desorption for the *C*-pore.

Point 2: A higher condensation pressure is required because the adsorbed layer has to be thick enough to leave a gas-like core small enough for condensation to occur in the *O*-pore.

Point 3: The evaporation from the *O*-pore is at a slightly greater pressure because it proceeds from two ends, but only from one end in the *C*-pore. Furthermore, the adsorbate near the closed end in the *C*-pore is more cohesive, and the desorption therefore occurs at a slightly lower pressure. This is illustrated by the radial density distribution at the closed end presented in Figure 2c for the points I and II labelled in Figure 2a where it can be clearly seen that the molecular packing at point II (higher loading in the *C*-pore) is more localised (sharper and higher maxima) and therefore more structured than that at point I in the *O*-pore.

Point 4: This is the consequence of the greater cohesiveness (average nearest neighbour separation is closer to the potential minimum) in the *C*-pore, which can therefore accommodate more molecules for a given pore volume.

The presence of a hysteresis loop in the *C*-pore demonstrates the failure of the classical Kelvin or Cohan form of equation. In our earlier work (Nguyen et al., 2013) we have shown a typical contour density plot in a closed end pore, and we noted a clear distinction between the adsorbed layers in adsorption and desorption. In adsorption, the layer thickness along the pore increases with pressure, but not as fast as the movement of the meniscus from the closed end to the pore mouth. On the other hand, for desorption, the thickness of the adsorbed layer along the pore wall remains constant as pressure is decreased. The loss of adsorbate mass is due to the withdrawal of the meniscus towards the closed end.

Let us first consider the mechanism of adsorption in the *C*-pore. At pressures before point *A* (Figure 2), molecular layering occurs on all surfaces, including the surface at the closed end. When point *A* is approached the interface between the dense adsorbate phase and the rarefied phase is developing and is fully developed with a curved interface at *A*. If we apply an equation of the Kelvin form to this interface we have:

$$RT \ln\left(\frac{P_A}{P_0}\right) = -\frac{\alpha_A}{r_A} \qquad (4)$$

where r_A is the mean radius of curvature at *A*. At point *B* on the sharp rise in the isotherm, where the pressure is greater than P_A, a Kelvin form of equation can also be written as:

$$RT \ln\left(\frac{P_B}{P_0}\right) = -\frac{\alpha_B}{r_B} \tag{5}$$

Since the adsorbed layer along the pore wall at point *B* is thicker than that at point *A*, the mean radius of curvature at *B* is therefore smaller than that at *A*. Thus in order for $P_A < P_B$ we must have:

$$\alpha_A > \alpha_B \tag{6}$$

This implies that the fluid is less cohesive as the interface advances away from the closed end (since a larger value of α means a more cohesive fluid) and the assumption of constant α is not correct because it would predict $P_B < P_A$, which contradicts the observed inequality. Thus, we can conclude that the adsorbate is more cohesive at the closed end, and the packing near the closed end is more structured with increased loading as seen in the corner-radial distribution shown in Figure 2c.

The classical equation is also incorrect for the desorption branch because the radius of curvature here is constant, since the adsorbed layer has constant thickness in the region of the co-existing adsorbed layer and rarefied gas of the *C*-pore, and therefore if the parameter α is constant, as assumed in the classical equation, the desorption branch would be vertical (instantaneous). This is, once again, not the case.

We have put forward a simple argument to show that the classical Kelvin type of equation with bulk-like parameters (surface tension and molar volume corresponding to a uniform bulk liquid) does not correctly describe adsorption and desorption in a *C*- pore. We now turn to a detailed discussion of how various parameters will affect the hysteresis.

3.2 Effects of Temperature

Figure 3 shows the isotherms and the density contour plots in the 3nm *O*-pore and 3nm *C*-pore for temperatures ranging from below the triple point to close to the critical hysteresis temperature. The four points noted above for the isotherms at 87K are again repeated for all these temperatures. We conclude that the Kelvin type of equation with constant bulk values for the parameters is not valid at any temperature.

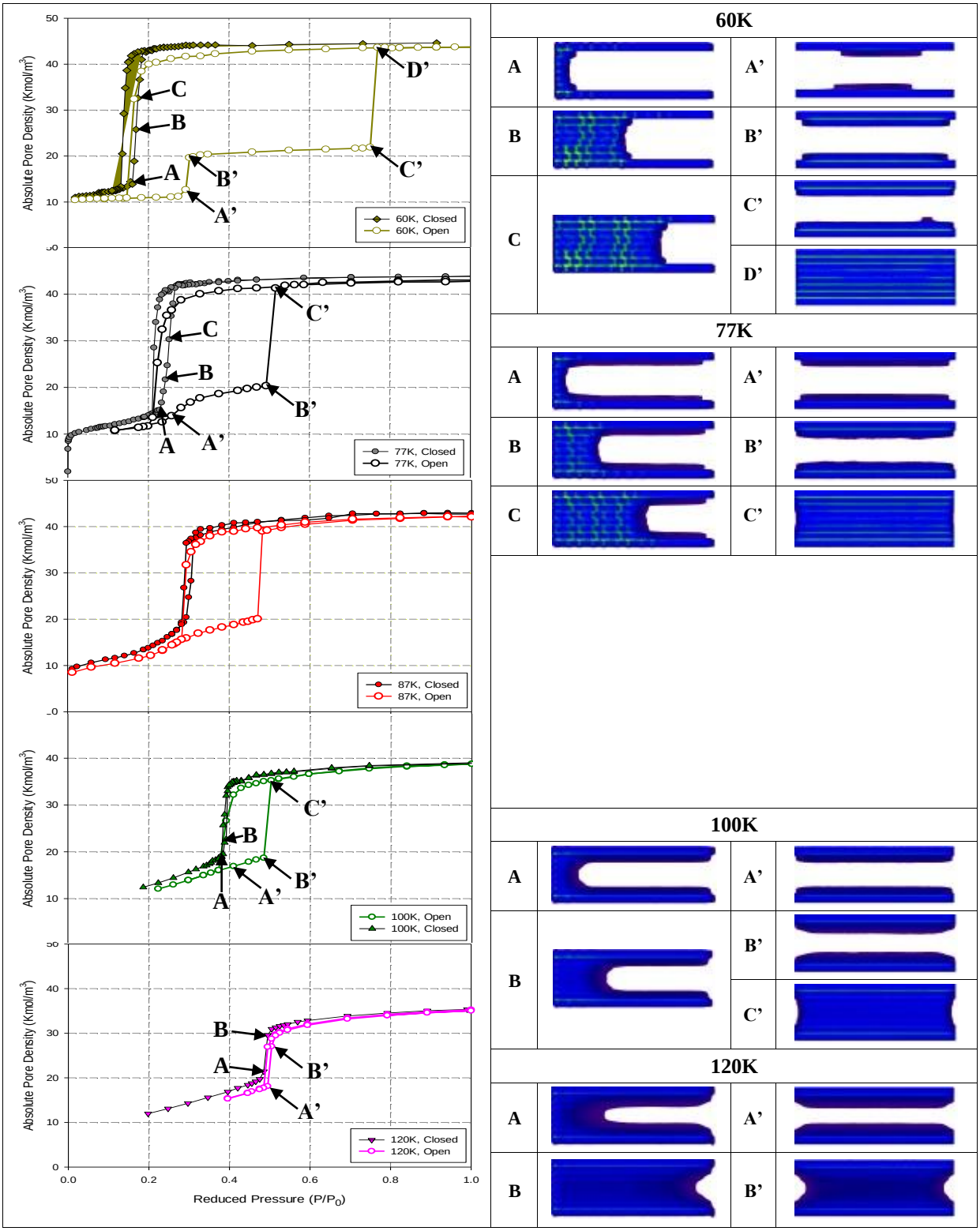

Figure 3: Effects of temperature on the argon adsorption isotherms in the *O*-pore and the *C*-pore; the pore widths are 3nm and lengths are 20nm; the 2D density profiles of the points are taken at the points labelled on the isotherms.

More additional features may be noted as follows.

1. Adsorption in the *O*-pore at 60K proceeds by step-wise molecular layering in which two distinct layers form on each wall, followed by a capillary condensation. This step-wise behaviour disappears as temperature is increased.
2. The reduced condensation pressure in the *O*-pore and the loading at which the condensation occurs are lowered as temperature is increased. This is due to the greater fluctuation of the undulatory interface (Zeng et al., 2014) at high T, causing condensation at a lower loading.
3. The reduced "condensation" pressure of the *C*-pore increases with temperature, in contrast to that in the *O*-pore, as explained in point 2 above. The different mechanism of adsorption in the C-pore accounts for this: i.e. as the temperature is increased, the thermal fluctuation increases and therefore it requires a higher chemical potential, i.e. P/P_0, to develop the meniscus at the closed end, and this is why greater pressure is required for the advance of the meniscus from the closed end to the pore mouth.
4. For both *O*-pore and *C*-pores, the reduced evaporation pressure increases with temperature because of the increased thermal fluctuation which favours the entropic component over the energy component.
5. The hysteresis loop for the *O*-pore is larger than that for the *C*-pore; they both decrease in area with temperature and the critical hysteresis temperatures of both pores are about the same viz: 120K, for this 3nm pore width (Zeng et al., 2014). It should be noted that the critical hysteresis temperature is pore size dependent.

3.3 Effects of Pore Dimensions (size, length)

The cohesiveness of the adsorbate in the *C*-pore can be substantiated with simulation results for *C*-pores of different length. Figure 4 shows the isotherms at 87K for 3nm *C*-pores with lengths of 10, 20 and 40nm. Figure 4a displays the isotherms as number of molecules versus the reduced pressure to demonstrate that the number of molecules required to fill the pore is proportional to the pore length. Moreover, for pores with different lengths, the meniscus is fully developed when the reduced pressure is around 0.3, after that the meniscus advances linearly with respect to pressure towards the pore mouth, as shown by the dashed line in Figure 4a. These *C*-pores have hysteresis loops of different size and different condensation and evaporation pressures. The isotherm for the shortest pore (10nm) is reversible and as the pore is lengthened the loop area increases; the condensation pressure shifts to the right and the evaporation pressure to the left, a feature not previously recognised in the literature. In

Figures 4b and c, the isotherms are shown as the surface excess and absolute pore density versus the reduced pressure, respectively. At low pressure, before condensation, the adsorption occurs through the layering on the pore walls, so the surface excess is the same irrespective of the pore length. However, because the ratio of surface areas/volume is decreased with the pore length, when the isotherm is presented as the absolute pore density, the density in the longer pore is smaller before condensation (Figure 4c).

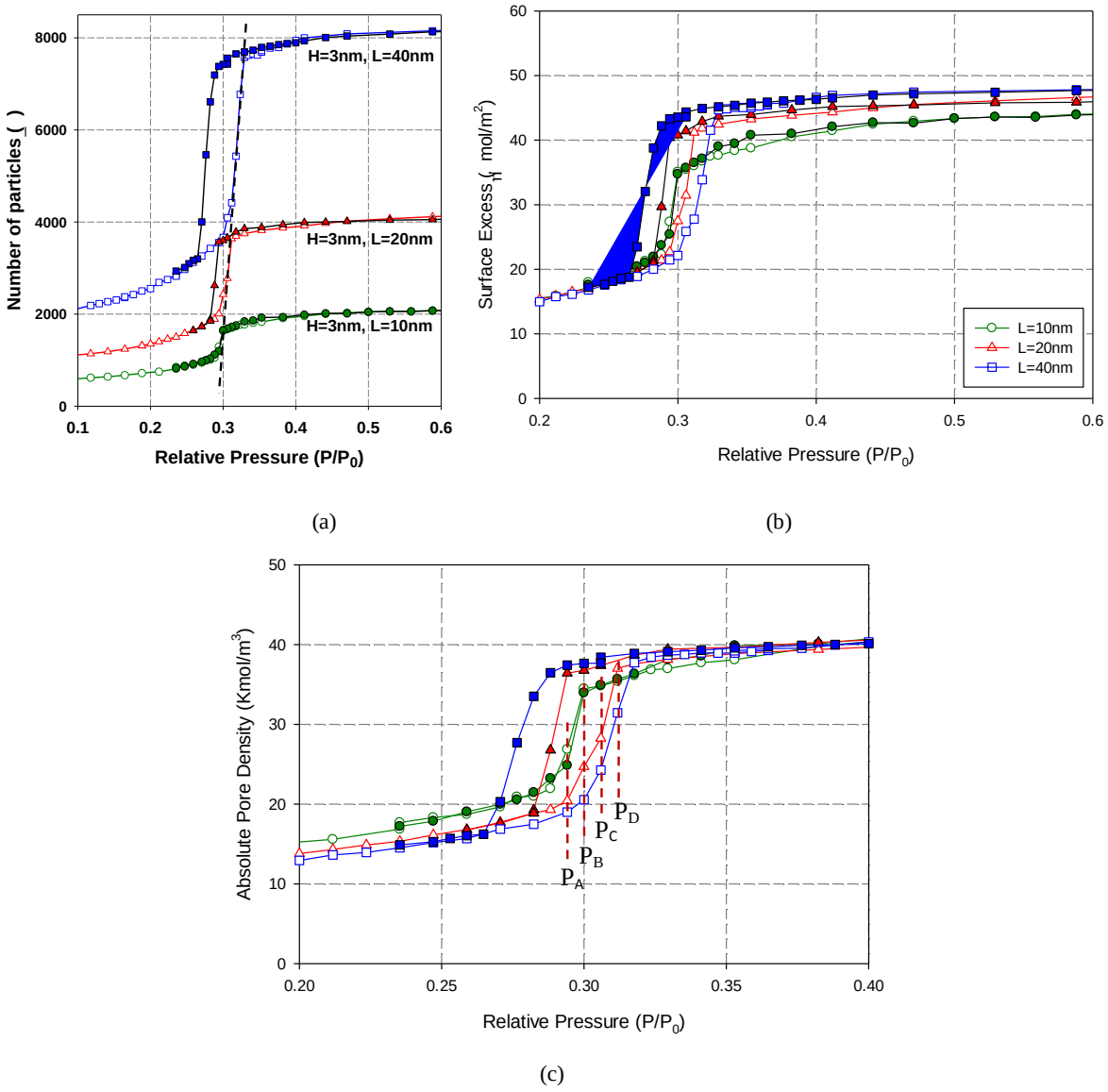

Figure 4: Effects of length on the argon adsorption isotherms in the *C*-pore; the pore widths are 3nm and the temperature is 87K.

To explain the shift of condensation pressure to higher values as the pore length is increased, we present, in Figure 5, the 2D-density profiles at the various pressures marked in Figure 4c. For pressures less than P_A, molecular layering occurs on all surfaces and a curved meniscus is

developed at the closed end. The distance of the meniscus from the closed end is the same for all pores at a given pressure. Another feature that is worth noting is that the increase in pore density with pressure is the same for all pores, and consequently for longer pores, a lower pressure is required for the meniscus to recede from the pore mouth to the closed end.

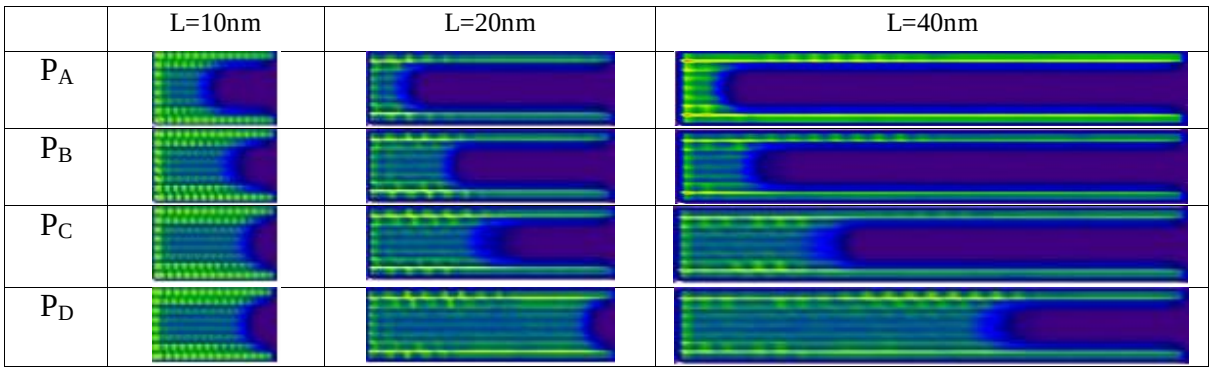

Figure 5: The 2D density Profiles at various pressures as marked in Figure 4c.

The adsorption isotherms for argon at 87K in the larger *O*-pore and *C*-pore, having widths of 4nm and length 20nm are presented in Figure 6a, together with the 2D density profiles in Figure 6b, at the points marked on the isotherms. As the pore width is increased, the hysteresis loop becomes wider, and all the characteristics noted above for 3nm pores are also observed here.

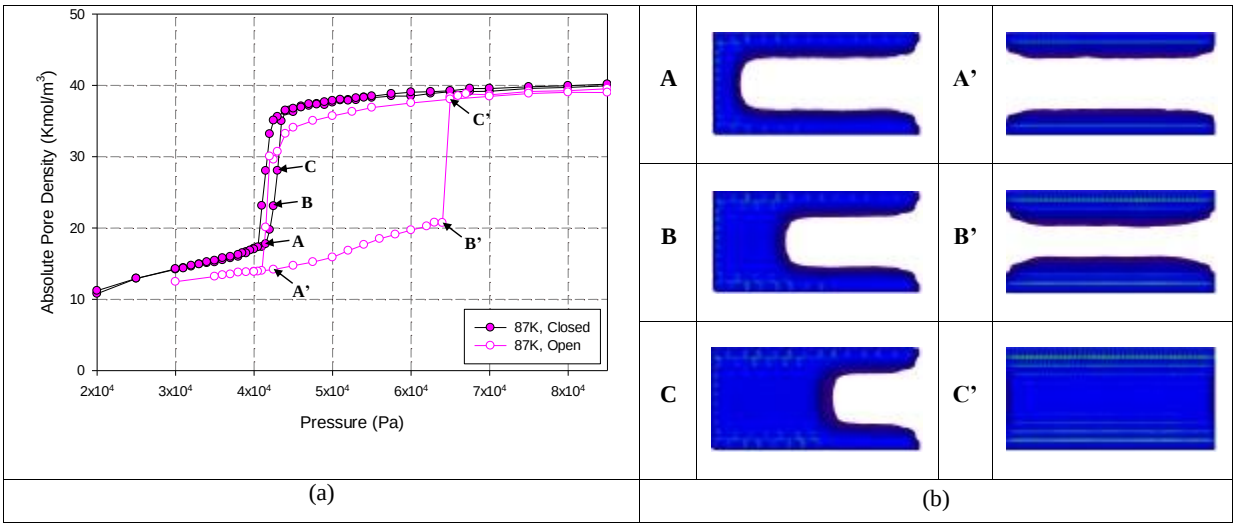

Figure 6: (a) adsorption isotherms and (b) 2D density profiles for argon at 87K in open end and closed end slit pores; the pore widths are 4nm and lengths 20nm.

3.4 Effects of Adsorbent Affinity

We have seen that the 3nm *C*-pores show hysteresis when the adsorbent potential field is equivalent to that of graphite. Reversible isotherms have been reported for closed end pores

when the interaction between adsorbate and adsorbent is weaker (Mistura et al., 2013); this raises the question of whether a reduction in this interaction is the reason for reversibility. Figure 7 shows the isotherms for a graphite-like (lamellar) surface in which the well depth (ε_{ss}/k) of an atom in the adsorbent is reduced from 28K to 10K. It is seen that hysteresis persists, and the size of the loop is not sensitive to the strength of the adsorbent field. However, when the well depth is further reduced to 5K, the hysteresis loop is significantly enlarged with a very sharp condensation. This is because when the solid affinity is so small, the enhancement of the solid-fluid interaction at the corner of the pore becomes less effective, and the adsorbent field in the closed end pore approaches that of an open end pore.

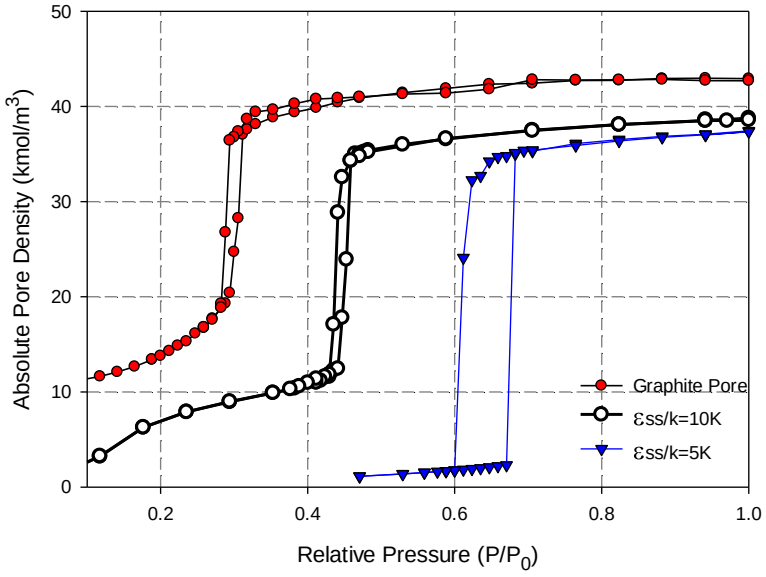

Figure 7: The comparison between the adsorption isotherms of argon at 87K in the closed end pore with graphite walls and reduced solid affinity of ε_{ss}/k=10K, 5K, with 3nm width and 20nm length.

3.5 Affinity of the closed end

When the closed end is treated as a hard wall, the isotherms resemble those for a pore with pore behaves like an open end pore as seen in Figure 8a. When ε_{ss}/k for the end section is set equal to 10K (whilst keeping a value of 28K for the pore walls) the evaporation pressure is even lower than that for the equivalent graphite pore as shown by the points marked as squares in Figure 8a. This can be explained by the different structure of the condensed fluid, and we illustrated it with the corner-radial density distributions (Figure 8b) and the snapshots (Figure 8c) at pressure P_I on the desorption branch as labelled in Figure 8a. From Figure 8b, it can be seen by reducing the affinity of the closed end ε_{ss}/k from graphite to 10K, the condensed fluids at the corner are less well structured, however, the snapshots show that the

fluids close to the open end is better structured, and this is accounted for the delayed evaporation of the pore with the weaker closed end. Once again, this observation here enhanced one of our arguments that the structure change of the condensed fluid contributes to the existence of hysteresis in closed end pore. For comparison, the snapshot at P_I for the fluids inside the pore with its closed end modelled as hard wall is shown in Figure 8c, and clearly two meniscuses are observed, which is similar to the case of open end pore, and for both the condensed fluids evaporated at higher pressure compared with the graphite pore.

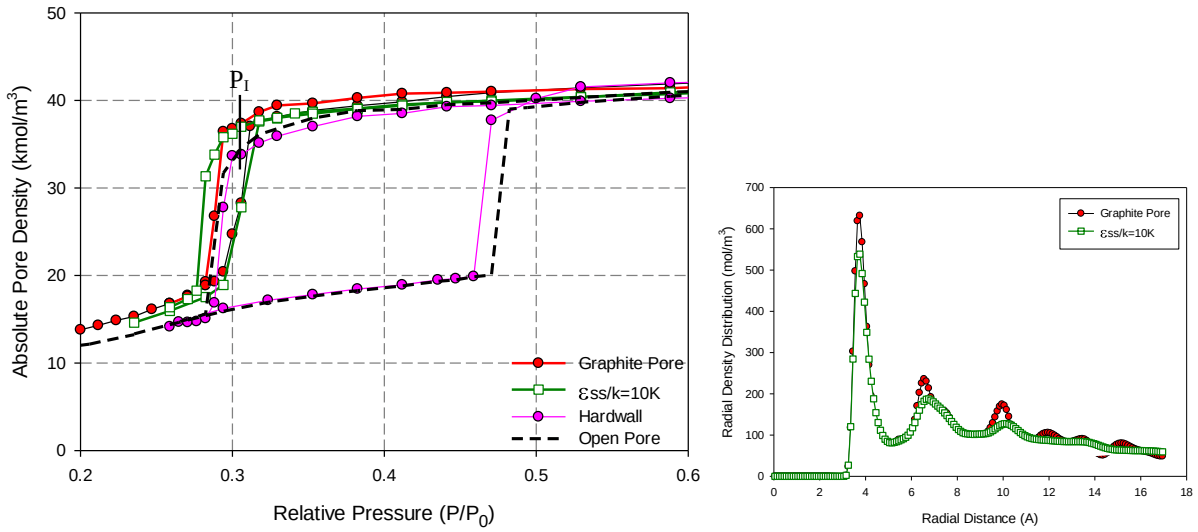

(a) (b)

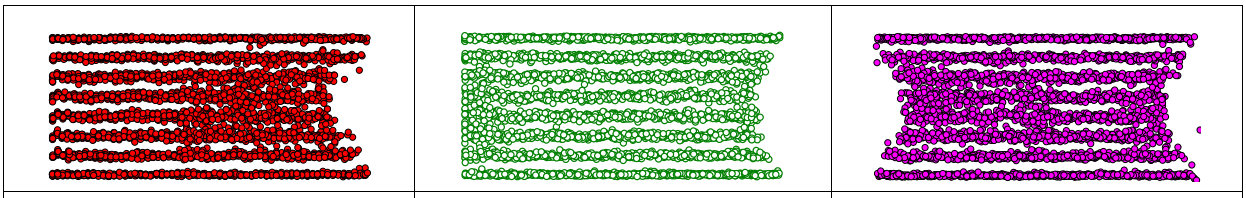

Graphite Pore	ε_{ss}/k=10K	Hard wall

(c)

Figure 8: (a) Isotherms for pores of 3nm and length 20nm with closed ends modelled as graphite walls (ε_{ss}/k = 28K; pentagon symbols), walls with (ε_{ss}/k=10K; squares) or hard walls (circles); (b) The corner-radial density distribution at P_I, of the pore with the closed end as graphite and ε_{ss}/k=10K, respectively; (c) The snapshots at P_I, of the pore with the closed end as graphite, ε_{ss}/k=10K and hard walls.

3.6 Effects of the potential energy profile

Finally we explore whether the form of the intermolecular energy could have an effect on the hysteresis loop. Instead of the LJ 12-6 for the fluid-fluid interaction and the Bojan-Steele 10-4 for the solid-fluid interaction, we used the Weeks-Chandler-Andersen (WCA) potential function to examine the effects of imposing an infinite repulsion when the separation distance between adsorbate molecules is less than the hard sphere cut-off as used in the WCA model. In Figure 9a, the comparison of potential profiles obtained with the WCA potential and LJ

potential is presented to show the cut-off and the well-depth of the WCA potential, compared to that of LJ potential, and their respective isotherms are shown in Figure 9b where we also show the effect of the hard sphere cut-off in the WCA potential. The hysteresis loops obtained with the WCA model are even larger than those for the LJ potential. We conclude that the changing the intermolecular potential profile in this way does not remove the hysteresis loop, and this casts doubt on DFT calculations because of the mean field approximation of this theory.

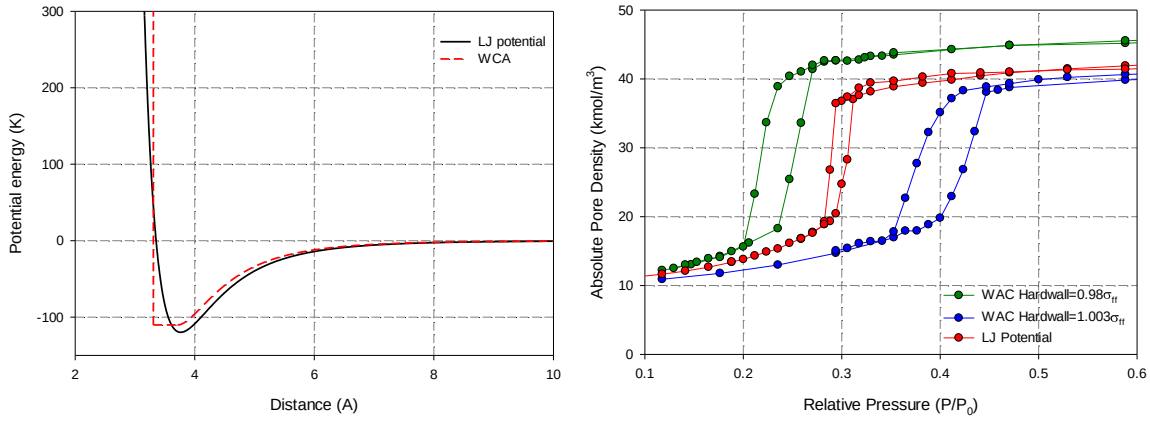

(a) (b)

Figure 9: (a) The comparison of the potential profile between the WCA potential (red curve, σ=3.375Å, ε/k=110.2K, the hard sphere d=0.98×3.375=3.3075Å) and LJ potential (black curve, σ=3.405Å, ε/k=119.8K); (b) the isotherms of the closed end pore of 3nm with length 20nm obtained LJ potential and WCA by using different distances for hard wall.

4 Conclusions

The assumption of bulk fluid parameters in the Kelvin description for adsorption and desorption in closed end slit pores has been shown to be invalid. We have confirmed that Monte Carlo simulations give hysteresis loops in closed end pores, and also examined the effects of various parameters on the form of the loops. The major findings from this study can be summarised as follows:

(1) For slit pores of similar dimensions, the open end pore has a larger hysteresis loop than the closed end pore, and its condensation pressure decreases with temperature, while the closed end pore shows the opposite trend.

(2) For closed end pores of the same pore width, the condensation and evaporation pressures shift to the right and the left respectively, as the pore length is increased, resulting in a wider hysteresis loop.

(3) The hysteresis loop shifts to a higher pressure for weaker surfaces, and its size is larger.

(4) The shape of the intermolecular potential energy (LJ or WCA with hard sphere cut-off) does not affect the appearance of the hysteresis loop.

Acknowledgement: This project is supported by the Australian Research Council

References

1. Ancilotto, F., Da Re, M., Grubisic, S., Hernando, A., Silvestrelli, P.L., Toigo, F., 2011. Grand Canonical Monte Carlo study of argon adsorption in aluminium nanopores. Molecular Physics 109, 2787-2796.
2. Bojan, M.J., Steele, W.A., 1988. Computer simulation of physisorption on a heterogeneous surface. Surface Science 199, L395-L402.
3. Bojan, M.J., Steele, W.A., 1993. Computer simulation of physical adsorption on stepped surfaces. Langmuir 9, 2569-2575.
4. Bojan, M.J., Steele, W.A., 1998. Computer simulations of the adsorption of xenon on stepped surfaces. Molecular Physics: An International Journal at the Interface Between Chemistry and Physics 95, 431 - 437.
5. Bruschi, L., Fois, G., Mistura, G., Sklarek, K., Hillebrand, R., Steinhart, M., Gosele, U., 2008. Adsorption hysteresis in self-ordered nanoporous alumina. Langmuir 24, 10936-10941.
6. Bruschi, L., Mistura, G., Liu, L., Lee, W., Gosele, U., Coasne, B., 2010. Capillary Condensation and Evaporation in Alumina Nanopores with Controlled Modulations. Langmuir 26, 11894-11898.
7. Coasne, B., Grosman, A., Ortega, C., Simon, M., 2002. Adsorption in Noninterconnected Pores Open at One or at Both Ends: A Reconsideration of the Origin of the Hysteresis Phenomenon. Physical Review Letters 88, 256102-256101-256102-256104.
8. Everett, D.H., Haynes, J.M., 1973. Capillarity and porous materials: Equilibrium properties. Colloid Science, 123-172.
9. Fan, C., Do, D.D., Nicholson, D., 2013. On the Hysteresis of Argon Adsorption in a Uniform Closed End Slit Pore. Journal of Colloid and Interface Science 405, 201-210.
10. Horikawa, T., Do, D.D., Nicholson, D., 2011. Capillary condensation of adsorbates in porous materials. Advances in Colloid and Interface Science 169, 40-58.
11. Johnson, J.K., Zollweg, J.A., Gubbins, K.E., 1993. The Lennard-Jones equation of state revisited. Molecular Physics: An International Journal at the Interface Between Chemistry and Physics 78, 591 - 618.
12. Mistura, G., Pozzato, A., Grenci, G., Bruschi, L., Tormen, M., 2013. Continuous adsorption in highly ordered porous matrices made by nanolithography. Nat Commun 4.
13. Mountain, R.D., Thirumalai, D., 1994. Quantitative measure of efficiency of Monte Carlo simulations. Physica A (Amsterdam) 210, 453-460.
14. Naumov, S., Valiullin, R., Kärger, J., Monson, P.A., 2009. Understanding adsorption and desorption processes in mesoporous materials with independent disordered channels. Physical Review E 80, 031607-031601-031607-031609.
15. Nguyen, P.T.M., Do, D.D., Nicholson, D., 2013. On the Irreversibility of the Adsorption Isotherm in a Closed-End Pore. Langmuir 29, 2927-2934.
16. Parry, A.O., Rascon, C., Wilding, N.B., Evans, R., 2007. Condensation in a capped capillary is a continuous critical phenomenon. Physical Review Letters 98.
17. Puibasset, J.l., 2009. Monte-Carlo Multiscale Simulation Study of Argon Adsorption/Desorption Hysteresis in Mesoporous Heterogeneous Tubular Pores like MCM-41 or Oxidized Porous Silicon. Langmuir 25, 903-911.
18. Roth, R., Parry, A.O., 2011. Drying in a capped capillary. Molecular Physics 109, 1159-1167.
19. Sarkisov, L., Monson, P.A., 2001. Modeling of adsorption and desorption in pores of simple geometry using molecular dynamics. Langmuir 17, 7600-7604.
20. Thommes, M., 2004. Physical adsorption characterization of ordered and amorphous mesoporous materials., in: Lu, G., Zhao, X.S. (Eds.), Nanoporous Materials, Science & Engineering Imperial College Press, London, pp. 317-364.
21. Wallacher, D., Künzner, N., Kovalev, D., Knorr, N., Knorr, K., 2004. Capillary Condensation in Linear Mesopores of Different Shape. Physical Review Letters 92, 195704-195701-195704-195704.
22. Zeng, Y., Fan, C., Do, D.D., Nicholson, D., 2014. Condensation and Evaporation in Slit-Shaped Pores: Effects of Adsorbate Layer Structure and Temperature. The Journal of Physical Chemistry C.